Considerations in the Calculation of Vertical Velocity in Three-Dimensional Circulation Models

Richard A. Luettich, Jr.
University of North Carolina at Chapel Hill
Institute of Marine Sciences
Morehead City, NC, USA 28557

Julia C. Muccino
Department of Civil and Environmental Engineering
Arizona State University
Tempe, AZ, USA 85287

Michael G. G. Foreman
Department of Fisheries and Oceans
Institute of Ocean Sciences
Sidney, British Columbia, CANADA V8L 4B2

Submitted to: *Journal of Atmospheric and Oceanic Technology*
Date: January 8, 2002

1. Abstract

The vertical velocity, w, in three-dimensional circulation models is typically computed from the three-dimensional continuity equation assuming that the depth-varying horizontal velocity field was calculated earlier in the solution sequence. Computing w in this way appears to require the solution of an over-determined system since the continuity equation is first order, yet w must satisfy two boundary conditions (one at the free surface and one at the bottom). At least three methods have been previously proposed to compute w: (i) the “traditional” method that solves the continuity equation with the bottom boundary condition and ignores the free surface boundary condition, (ii) a “vertical derivative” method that solves the vertical derivative of the continuity equation using both boundary conditions and (iii) an “adjoint” approach that minimizes a cost functional comprised of residuals in the continuity equation and in both boundary conditions. The latter solution is equivalent to the "traditional" solution plus a correction that increases linearly over the depth and is proportional to the misfit between the "traditional" solution at the surface and the surface boundary condition.

In this paper we show that the "vertical derivative" method yields inaccurate and physically inconsistent results if it is discretized as has been previously proposed. However, if properly discretized the "vertical derivative" method is equivalent to the “adjoint” method if the cost function is weighted to exactly satisfy the boundary conditions. Furthermore, if the horizontal flow field satisfies the depth-integrated continuity equation locally, one of the boundary conditions is redundant and w obtained from the "traditional" method should match the free surface boundary condition. In this case, the “traditional,” “adjoint” and properly discretized “vertical derivative” approaches yield the same results for w. If the horizontal flow field is not locally mass conserving, the mass conservation error is transferred into the solution for w. This is particularly important for models that do not guarantee local mass conservation, such as some finite element models.

2. Introduction

This paper investigates the merits of different approaches for calculating vertical velocity fields by solving the three-dimensional continuity equation, assuming the horizontal velocity fields are known.

In typical three-dimensional circulation models [e.g., FUNDY (*Lynch and Werner*, 1987), POM (*Blumberg and Mellor*, 1987), QUODDY (*Lynch and Werner*, 1991, *Lynch and Naimie*, 1993), ROMS (*Haidvogel and Beckmann*, 1999)] the vertical velocity is determined from the three-dimensional continuity equation:

$$\frac{\partial w}{\partial z} = -\nabla \bullet \mathbf{V} \tag{1}$$

where $\mathbf{V}(x, y, z, t)$ is the horizontal velocity with components $(u(x, y, z, t), v(x, y, z, t))$, and $w(x, y, z, t)$ is the vertical velocity. Here (x, y) are the horizontal coordinates, z is the vertical coordinate (positive upward, $z = 0$ at the mean water surface), t is time and ∇ is the horizontal gradient operator. The kinematic boundary condition on vertical velocity at the bottom is:

$$w = -\mathbf{V} \bullet \nabla h = w_b \quad \text{at} \quad z = -h \tag{2a}$$

where $h(x, y)$ is the mean water depth. The analogous condition at the surface is:

$$w = \frac{\partial \eta}{\partial t} + \mathbf{V} \bullet \nabla \eta = w_s \quad \text{at} \quad z = \eta \tag{2b}$$

where $\eta(x, y, t)$ is the surface elevation. [Note, for future reference, w_b has been defined as the vertical velocity at the bottom as determined from the boundary condition and w_s has been defined as the vertical velocity at the surface as determined from the boundary condition.] Equations (1), (2a), (2b) are solved for w assuming that the horizontal velocity and surface elevations are known from a previous part of the model solution. The primary difficulty of solving these equations is that, together, they constitute an over-determined system of equations for the most general case;

that is, (1) is a *first* order equation that must be solved subject to *two* boundary conditions. As will be shown, in numerical schemes that are locally mass conserving, one of the boundary conditions becomes redundant and thus the system is not over-determined.

We will consider here two approaches to solving the over-determined system:

1. Solution of the vertical derivative of the continuity equation:

$$\frac{\partial^2 w_{vdc}}{\partial z^2} = -\frac{\partial}{\partial z}(\nabla \bullet \mathbf{V}) \tag{3}$$

   where w_{vdc} indicates vertical velocity computed using the this approach (henceforth, VDC). This is a second order differential equation and thus both boundary conditions can be satisfied (*Lynch and Naimie*, 1993).

2. Solution of the over-determined system in a "best fit" sense by admitting residuals in the first order continuity equation and both boundary conditions. An optimal solution is then sought that minimizes those residuals in a weighted least squared sense. Because this approach involves the adjoint of the continuity equation, we call it the "adjoint" approach (henceforth, ADJ). It will be described in more detail in Section 3.

A third approach, called the "traditional" approach (TRAD) simply neglects one of the boundary conditions; this approach will be shown here to be a component of ADJ.

Muccino et al. (1997) found that VDC and ADJ provide different vertical velocity fields regardless of resolution in the vertical or horizontal and that ADJ better approximates the analytic solution in a simple test problem than VDC. The objectives of this paper are to reconcile the numerical differences between VDC and ADJ and to make overall recommendations for the computation of vertical velocity in three-dimensional circulation models. Results are provided for tidally forced

circulation in a quarter annular test case and a wind, density and boundary forced circulation off the southwest coast of Vancouver Island.

3. A summary of the adjoint approach (ADJ)

ADJ admits residuals in the continuity equation (1) and the boundary conditions (2a) and (2b) at each horizontal node:

$$f(z) = \frac{\partial w}{\partial z} + \nabla \bullet \mathbf{V} \tag{4a}$$

$$i_b = w + \mathbf{V} \bullet \nabla h \qquad \text{at} \quad z = -h \tag{4b}$$

$$i_s = w - \frac{\partial \eta}{\partial t} - \mathbf{V} \bullet \nabla \eta \qquad \text{at} \quad z = \eta \tag{4c}$$

A cost functional, which is formed from the squares of these residuals is defined:

$$I = \frac{W_f}{H} \int_{-h}^{\eta} \{f\}^2 dz + W_b \{i_b\}^2 + W_s \{i_s\}^2 \tag{5}$$

where W_f, W_b and W_s are constant weights and $H(x, y, t) = h(x, y) + \eta(x, y, t)$ is the total water depth and is included in the denominator of the first term to normalize the vertical integral and also to maintain dimensional consistency. The weights are defined as the inverses of the covariances of the residuals:

$$W_f = \frac{1}{C_f}, \qquad W_b = \frac{1}{C_b}, \qquad W_s = \frac{1}{C_s} \tag{6}$$

where the covariances are defined as:

$$C_f = \langle f^2 \rangle, \qquad C_b = \langle i_b^2 \rangle, \qquad C_s = \langle i_s^2 \rangle \tag{7}$$

and $\langle\ \rangle$ indicates expected value. Thus the dimensions of W_f, W_b and W_s are T^2, T^2/L^2 and T^2/L^2, respectively. We will assume that $W_b = W_s$. Additionally, given that only the relative

values of the weights is significant (not the absolute values of the weights themselves) we set $W_b = W_s = 1$ without further loss of generality. Thus, (5) can be written:

$$I = \frac{W_f}{H}\int_{-h}^{\eta} \{f\}^2 dz + \{i_b\}^2 + \{i_s\}^2 \tag{8}$$

The adjoint solution, w_{adj}, minimizes I and can be shown to be:

$$w_{adj}(z) = w_{trad}(z) + w_c(z), \quad w_c(z) = (w_s - w_{trad}(\eta))\frac{W_f/H^2 + (h+z)/H}{2W_f/H^2 + 1} \tag{9}$$

where w_{trad} is the "traditional solution" to the governing equation (1) and the bottom boundary condition (2a). [For mathematical details leading to (9) see *Muccino* (1997); for a similar derivation using "representers," see Appendix A of *Muccino and Bennett* (2001)] Thus, the adjoint solution is a sum of w_{trad} and a correction that is linear in z and proportional to the misfit between the traditional solution evaluated at the surface and the surface boundary condition. In the limit of $W_f/H^2 = 0$ (that is, no weight given to the three-dimensional continuity equation in I), the correction reduces to:

$$w_c(z) = (w_s - w_{trad}(\eta))\frac{h+z}{H} \quad \text{for} \quad W_f/H^2 = 0 \tag{10}$$

In this case, the correction is zero at the bottom and equal to the surface boundary condition misfit of the traditional solution at the surface. Consequently, the correction causes the adjoint solution to satisfy both boundary conditions exactly although it may diminish the mass conserving properties of the solution. In the limit of $W_f/H^2 \to \infty$, (that is, no weight given to the boundary conditions in I) (9) reduces to:

$$w_c(z) = \frac{w_s - w_{trad}(\eta)}{2} \quad \text{for} \quad W_f \to \infty \tag{11}$$

In this case, the correction approaches a constant (half the surface boundary condition misfit of the

traditional solution) over the depth. This distributes any error evenly between the surface and bottom boundary conditions, but has no impact on the mass conserving property of the solution. Clearly, intermediate values of W_f/H^2 generate corrections that fall between these limits. These observations are illustrated in Figure 1, which shows the correction, normalized by the surface boundary condition misfit:

$$w_n(z) = \frac{w_c(z)}{w_s - w_{trad}(\eta)} = \frac{W_f/H^2 + (h+z)/H}{2W_f/H^2 + 1} \tag{12}$$

for various values of W_f/H^2.

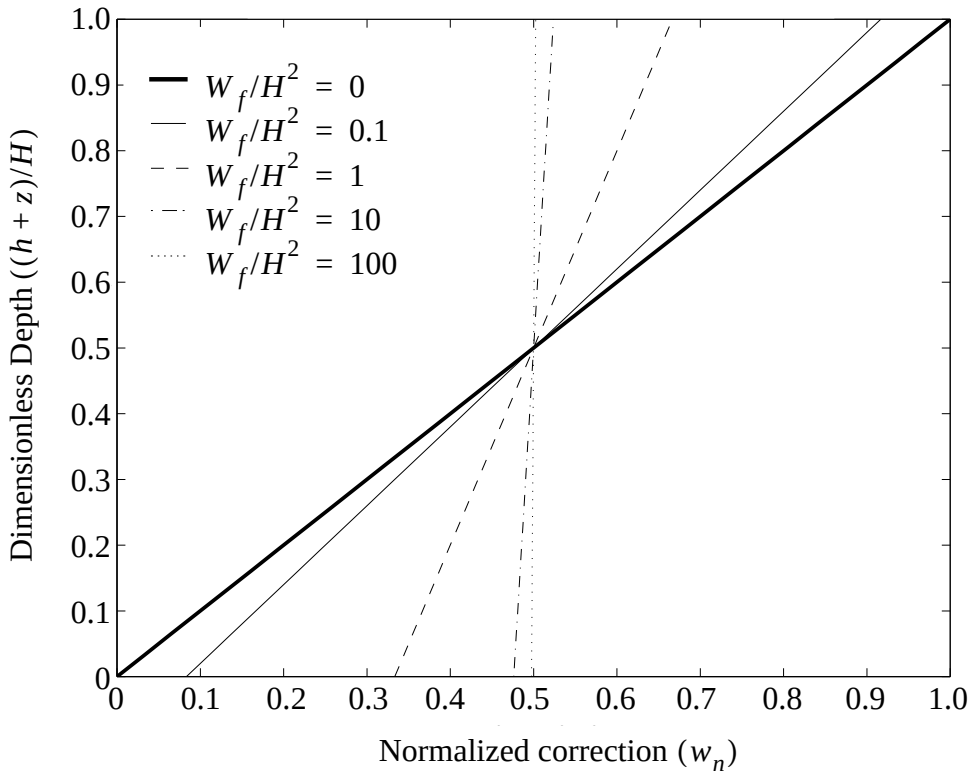

Figure 1. Normalized ADJ correction profiles for a range of W_f/H^2. For $W_f/H^2 = 0$, the normalized correction ranges from 0.0 at the bottom to 1.0 at the top. For large W_f/H^2, the normalized misfit approaches a constant value of 0.5.

4. Numerical Implementation

Two approaches to determining the vertical velocity have been described and these will now be tested numerically. A vertical sequence of three nodes indicated by subscripts $i-1$, i and $i+1$ will be used, as shown in Figure 2. Superscripts $-$ and $+$ indicate quantities evaluated over the intervals $\{i-1, i\}$ and $\{i, i+1\}$, respectively, (e.g., $\Delta z^{+} = z^{i+1} - z^{i}$).

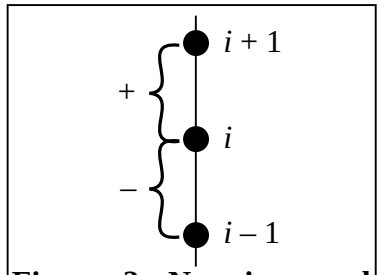

Figure 2. Notation used for vertical discretization

4.1 Discretization of VDC

Using centered finite difference, the LHS of (3) can be discretized:

$$\frac{\partial^2 w_{vdc}}{\partial z^2} = \frac{\partial}{\partial z}\left(\frac{\partial w_{vdc}}{\partial z}\right) \approx \frac{\left(\frac{\partial w_{vdc}}{\partial z}\right)^{+} - \left(\frac{\partial w_{vdc}}{\partial z}\right)^{-}}{\frac{1}{2}(\Delta z^{+} + \Delta z^{-})}$$

$$= \frac{\left(\frac{w_{vdc}^{i+1} - w_{vdc}^{i}}{\Delta z^{+}}\right) - \left(\frac{w_{vdc}^{i} - w_{vdc}^{i-1}}{\Delta z^{-}}\right)}{\frac{1}{2}(\Delta z^{+} + \Delta z^{-})}$$

$$= \frac{2}{(\Delta z^{+} + \Delta z^{-})}\left[\frac{w_{vdc}^{i+1}}{\Delta z^{+}} - w_{vdc}^{i}\left(\frac{1}{\Delta z^{+}} + \frac{1}{\Delta z^{-}}\right) + \frac{w_{vdc}^{i-1}}{\Delta z^{-}}\right] \tag{13}$$

and the RHS of (3) can be discretized:

$$-\frac{\partial}{\partial z}(\nabla \bullet \mathbf{V}) \approx -\frac{(\nabla \bullet \mathbf{V})^{+} - (\nabla \bullet \mathbf{V})^{-}}{\frac{1}{2}(\Delta z^{+} + \Delta z^{-})}$$

$$= -\frac{2}{(\Delta z^{+} + \Delta z^{-})}\frac{1}{2}\{[(\nabla \bullet \mathbf{V})^{i+1} + (\nabla \bullet \mathbf{V})^{i}] - [(\nabla \bullet \mathbf{V})^{i} + (\nabla \bullet \mathbf{V})^{i-1}]\} \tag{14}$$

Combining (13) and (14) yields:

$$\frac{w_{vdc}^{i+1}}{\Delta z^{+}} - w_{vdc}^{i}\left(\frac{1}{\Delta z^{+}} + \frac{1}{\Delta z^{-}}\right) + \frac{w_{vdc}^{i-1}}{\Delta z^{-}} = -\frac{1}{2}\{[(\nabla \bullet \mathbf{V})^{i+1} + (\nabla \bullet \mathbf{V})^{i}]^{+} - [(\nabla \bullet \mathbf{V})^{i} + (\nabla \bullet \mathbf{V})^{i-1}]^{-}\} \tag{15}$$

where the '+' and '-' have been added to the two terms inside the curly brackets of (15) as a reminder that the first group in square brackets is evaluated over the interval $\{i, i+1\}$ and the second group is evaluated over the interval $\{i-1, i\}$.

The LHS of (15) is tridiagonal and efficiently solved using a tridiagonal solver like the Thomas algorithm. The RHS of (15) requires the evaluation of the horizontal velocity on level coordinate surfaces. Most three-dimensional circulation models use stretched or terrain following coordinates in which the vertical dimension is transformed from $-h < z < \eta$ to $b < \sigma < a$, where a and b are arbitrary constants (e.g., $a = 1$, $b = 0$):

$$\sigma = a + \frac{(a-b)(z-\eta)}{H} \tag{16}$$

Derivatives in the terrain following coordinate system are related to derivatives in the level coordinate system using the chain rule:

$$\nabla \bullet \mathbf{V} = \nabla_{\sigma} \bullet \mathbf{V} - \frac{(a-b)}{H}\left[\frac{(\sigma-b)}{(a-b)}\nabla\eta + \frac{(\sigma-a)}{(a-b)}\nabla h\right] \bullet \frac{\partial \mathbf{V}}{\partial \sigma} \tag{17a}$$

$$\frac{\partial}{\partial z} = \frac{(a-b)}{H}\frac{\partial}{\partial \sigma} \tag{17b}$$

where ∇ indicates horizontal derivatives on a level surface and ∇_{σ} indicates horizontal derivatives on a stretched surface. Using (17a) and (17b) to expand terms on the RHS of (15) gives:

$$[(\nabla\bullet\mathbf{V})^{i+1}]^{+} = (\nabla_{\sigma}\bullet\mathbf{V})^{i+1} - \frac{(a-b)}{H}\left[\left(\frac{\sigma^{i+1}-b}{a-b}\right)\nabla\eta + \left(\frac{\sigma^{i+1}-a}{a-b}\right)\nabla h\right]\bullet\left(\frac{\mathbf{V}^{i+1}-\mathbf{V}^{i}}{\Delta\sigma^{+}}\right) \quad (18a)$$

$$[(\nabla\bullet\mathbf{V})^{i}]^{+} = (\nabla_{\sigma}\bullet\mathbf{V})^{i} - \frac{(a-b)}{H}\left[\left(\frac{\sigma^{i}-b}{a-b}\right)\nabla\eta + \left(\frac{\sigma^{i}-a}{a-b}\right)\nabla h\right]\bullet\left(\frac{\mathbf{V}^{i+1}-\mathbf{V}^{i}}{\Delta\sigma^{+}}\right) \quad (18b)$$

$$[(\nabla\bullet\mathbf{V})^{i}]^{-} = (\nabla_{\sigma}\bullet\mathbf{V})^{i} - \frac{(a-b)}{H}\left[\left(\frac{\sigma^{i}-b}{a-b}\right)\nabla\eta + \left(\frac{\sigma^{i}-a}{a-b}\right)\nabla h\right]\bullet\left(\frac{\mathbf{V}^{i}-\mathbf{V}^{i-1}}{\Delta\sigma^{-}}\right) \quad (18c)$$

$$[(\nabla\bullet\mathbf{V})^{i-1}]^{-} = (\nabla_{\sigma}\bullet\mathbf{V})^{i-1} - \frac{(a-b)}{H}\left[\left(\frac{\sigma^{i-1}-b}{a-b}\right)\nabla\eta + \left(\frac{\sigma^{i-1}-a}{a-b}\right)\nabla h\right]\bullet\left(\frac{\mathbf{V}^{i}-\mathbf{V}^{i-1}}{\Delta\sigma^{-}}\right) \quad (18d)$$

Substituting (18a) through (18d) and recognizing that $\Delta z = H\Delta\sigma/(a-b)$ yields:

$$\begin{aligned}
&\frac{w_{vdc}^{i+1}}{\Delta\sigma^{+}} - w_{vdc}^{i}\left(\frac{1}{\Delta\sigma^{+}} + \frac{1}{\Delta\sigma^{-}}\right) + \frac{w_{vdc}^{i-1}}{\Delta\sigma^{-}} \\
&= -\frac{1}{2}\Bigg\{\frac{H}{(a-b)}[(\nabla_{\sigma}\bullet\mathbf{V})^{i+1} + (\nabla_{\sigma}\bullet\mathbf{V})^{i}]^{+} - \frac{H}{(a-b)}[(\nabla_{\sigma}\bullet\mathbf{V})^{i} + (\nabla_{\sigma}\bullet\mathbf{V})^{i-1}]^{-} \\
&\quad - \left[\frac{(\sigma^{i+1}-b)}{(a-b)}\nabla\eta + \frac{(\sigma^{i+1}-a)}{(a-b)}\nabla h\right]\bullet\left(\frac{\mathbf{V}^{i+1}-\mathbf{V}^{i}}{\Delta\sigma^{+}}\right) \\
&\quad - \left[\frac{(\sigma^{i}-b)}{(a-b)}\nabla\eta + \frac{(\sigma^{i}-a)}{(a-b)}\nabla h\right]\bullet\left[\left(\frac{\mathbf{V}^{i+1}-\mathbf{V}^{i}}{\Delta\sigma^{+}}\right) - \left(\frac{\mathbf{V}^{i}-\mathbf{V}^{i-1}}{\Delta\sigma^{-}}\right)\right] \\
&\quad + \left[\frac{(\sigma^{i-1}-b)}{(a-b)}\nabla\eta + \frac{(\sigma^{i-1}-a)}{(a-b)}\nabla h\right]\bullet\left(\frac{\mathbf{V}^{i}-\mathbf{V}^{i-1}}{\Delta\sigma^{-}}\right)\Bigg\}
\end{aligned} \quad (19)$$

In practice, the horizontal derivatives $[(\nabla_{\sigma}\bullet\mathbf{V})^{i}]^{+} = [(\nabla_{\sigma}\bullet\mathbf{V})^{i}]^{-}$ and therefore (19) reduces to:

$$\frac{w_{vdc}^{i+1}}{\Delta\sigma^{+}} - w_{vdc}^{i}\left(\frac{1}{\Delta\sigma^{+}} + \frac{1}{\Delta\sigma^{-}}\right) + \frac{w_{vdc}^{i-1}}{\Delta\sigma^{-}}$$

$$= -\frac{1}{2}\left\{\frac{H}{(a-b)}\left[(\nabla_{\sigma}\bullet\mathbf{V})^{i+1} - (\nabla_{\sigma}\bullet\mathbf{V})^{i-1}\right]\right.$$

$$-\left[\frac{(\sigma^{i+1}-b)}{(a-b)}\nabla\eta + \frac{(\sigma^{i+1}-a)}{(a-b)}\nabla h\right]\bullet\left(\frac{\mathbf{V}^{i+1}-\mathbf{V}^{i}}{\Delta\sigma^{+}}\right)$$

$$-\left[\frac{(\sigma^{i}-b)}{(a-b)}\nabla\eta + \frac{(\sigma^{i}-a)}{(a-b)}\nabla h\right]\bullet\left[\left(\frac{\mathbf{V}^{i+1}-\mathbf{V}^{i}}{\Delta\sigma^{+}}\right) - \left(\frac{\mathbf{V}^{i}-\mathbf{V}^{i-1}}{\Delta\sigma^{-}}\right)\right]$$

$$\left.+\left[\frac{(\sigma^{i-1}-b)}{(a-b)}\nabla\eta + \frac{(\sigma^{i-1}-a)}{(a-b)}\nabla h\right]\bullet\left(\frac{\mathbf{V}^{i}-\mathbf{V}^{i-1}}{\Delta\sigma^{-}}\right)\right\} \qquad (20)$$

where no ambiguity is introduced by dropping the + and - superscripts on the remaining horizontal velocity gradient terms.

An alternative expression for w_{vdc} is obtained from (15) if it is assumed that the horizontal derivatives $[(\nabla\bullet\mathbf{V})^{i}]^{+} = [(\nabla\bullet\mathbf{V})^{i}]^{-}$. Using the chain rule, (15) reduces to:

$$\frac{w_{vdc}^{i+1}}{\Delta\sigma^{+}} - w_{vdc}^{i}\left(\frac{1}{\Delta\sigma^{+}} + \frac{1}{\Delta\sigma^{-}}\right) + \frac{w_{vdc}^{i-1}}{\Delta\sigma^{-}}$$

$$= -\frac{1}{2}\left\{\frac{H}{(a-b)}\left[(\nabla_{\sigma}\bullet\mathbf{V})^{i+1} - (\nabla_{\sigma}\bullet\mathbf{V})^{i-1}\right]\right.$$

$$-\left[\frac{(\sigma^{i+1}-b)}{(a-b)}\nabla\eta + \frac{(\sigma^{i+1}-a)}{(a-b)}\nabla h\right]\bullet\left(\frac{\mathbf{V}^{i+1}-\mathbf{V}^{i}}{\Delta\sigma^{+}}\right)$$

$$\left.+\left[\frac{(\sigma^{i-1}-b)}{(a-b)}\nabla\eta + \frac{(\sigma^{i-1}-a)}{(a-b)}\nabla h\right]\bullet\left(\frac{\mathbf{V}^{i}-\mathbf{V}^{i-1}}{\Delta\sigma^{-}}\right)\right\} \qquad (21)$$

It is clear that (20) and (21) are identical only if $\left[\frac{\partial\mathbf{V}}{\partial\sigma}\right]^{+} = \left[\frac{\partial\mathbf{V}}{\partial\sigma}\right]^{-}$. Previous investigators (*Lynch and Naimie,* 1993; *Muccino et al.,* 1997) have used an expression for w_{vdc} that is equivalent to

(21). However, results from *Muccino et al.* (1997) show that these values of w_{vdc} do not agree with vertical velocities obtained with ADJ. Below, we demonstrate that (20) does yield values that are essentially identical to ADJ, while (21) yields significantly inferior estimates of vertical velocity.

4.2 Discretization of ADJ

Recall, the adjoint solution, (9), consists of the sum of the traditional solution w_{trad} (the solution of the governing equation using the bottom boundary condition and neglecting the surface boundary condition) plus a correction. Thus, the numerical solution proceeds by first finding w_{trad} by discretizing (1):

$$\frac{w_{trad}^{i} - w_{trad}^{i-1}}{\Delta z^{-}} = -\frac{1}{2}[(\nabla \bullet \mathbf{V})^{i} + (\nabla \bullet \mathbf{V})^{i-1}] \tag{22}$$

Using the chain rule, this becomes:

$$\begin{aligned}\frac{w_{trad}^{i} - w_{trad}^{i-1}}{\Delta \sigma^{-}} = -\frac{1}{2}\Bigg\{ & \frac{H}{a-b}[(\nabla_{\sigma}\bullet\mathbf{V})^{i} + (\nabla_{\sigma}\bullet\mathbf{V})^{i-1}] \\ & -\left[\frac{(\sigma^{i}-b)}{(a-b)}\nabla\eta + \frac{(\sigma^{i}-a)}{(a-b)}\nabla h\right]\bullet\left[\frac{\mathbf{V}^{i}-\mathbf{V}^{i-1}}{\Delta\sigma^{-}}\right] \\ & -\left[\frac{(\sigma^{i-1}-b)}{(a-b)}\nabla\eta + \frac{(\sigma^{i-1}-a)}{(a-b)}\nabla h\right]\bullet\left[\frac{\mathbf{V}^{i}-\mathbf{V}^{i-1}}{\Delta\sigma^{-}}\right]\end{aligned} \tag{23}$$

The calculation is initiated using the bottom boundary condition, and then marched up the water column; no matrix solver is required. Once w_{trad} is known, w_c is easily computed algebraically and added to w_{trad} to yield the adjoint solution, w_{adj}.

4.3 Comparison of VDC and ADJ

Consider VDC first. The second order equation should admit, in addition to the solution of the associated first order equation, terms that are linear and constant in z. For example, suppose the vertical velocity that satisfies the first order equation (1) is:

$$w(z) = g(z) \tag{24a}$$

Consider a different vertical velocity field with addition terms, linear and constant in z:

$$w(z) = g(z) + c_1 z + c_2 \tag{24b}$$

where c_1 and c_2 are constants. The second derivatives of both (24a) and (24b) are:

$$\frac{\partial w^2}{\partial z^2} = \frac{\partial g^2}{\partial z^2} \tag{25}$$

Thus, the additional terms in the vertical velocity are transparent in VDC. Furthermore, since the VDC solution is forced to satisfy both boundary conditions, these terms take on a form such that $w(z)$ satisfies both boundary conditions.

Now consider ADJ with $W_f/H^2 = 0$. Equation (10) can be written in the form of (24b), where:

$$g(z) = w_{trad}(z) + (w_s - w_{trad}(\eta))\frac{z}{H} + (w_s - w_{trad}(\eta))\frac{h}{H} \tag{26}$$

and therefore:

$$c_1 = \frac{(w_s - w_{trad}(\eta))}{H}, \qquad c_2 = (w_s - w_{trad}(\eta))\left(\frac{h}{H}\right). \tag{27}$$

Thus, VDC and ADJ with $W_f/H^2 = 0$ should theoretically yield the same vertical velocity solution. Indeed, this equivalence is found numerically when (20) is used for the VDC solution

although it does not occur when (21) is used for the VDC solution. This is demonstrated below using two different test problems.

5. Quarter Annular Harbor Test Case

We begin numerical tests in a quarter annular harbor with quadratic bathymetry and periodic boundary forcing; the analytic vertical velocity for this problem is given in *Muccino et al.* (1997) and thus serves as a useful starting point for comparing the accuracy of these approaches. That solution is repeated in the Appendix for convenience.

The geometry of the quarter annular harbor is as in *Muccino et al.* (1997) and is shown in Figure 3. The boundaries at $r = r_1 = 4\text{x}10^4\text{m}$, $\theta = 0$, and $\theta = \pi/2$ are no-flow boundaries. The open boundary, located at $r = r_2 = 1\text{x}10^5\text{m}$, is forced by an M_2 tide with frequency $\omega = 1.405\times10^{-4}\text{s}^{-1}$ and amplitude $\eta_0 = 0.10\ \text{m}$. The bathymetry of the harbor, as shown in Figure 3b, is quadratic in r and constant in θ, such that $h = h_0 r^2$, where $h_0 = 6.25\times10^{-9}\ \text{m}^{-1}$.

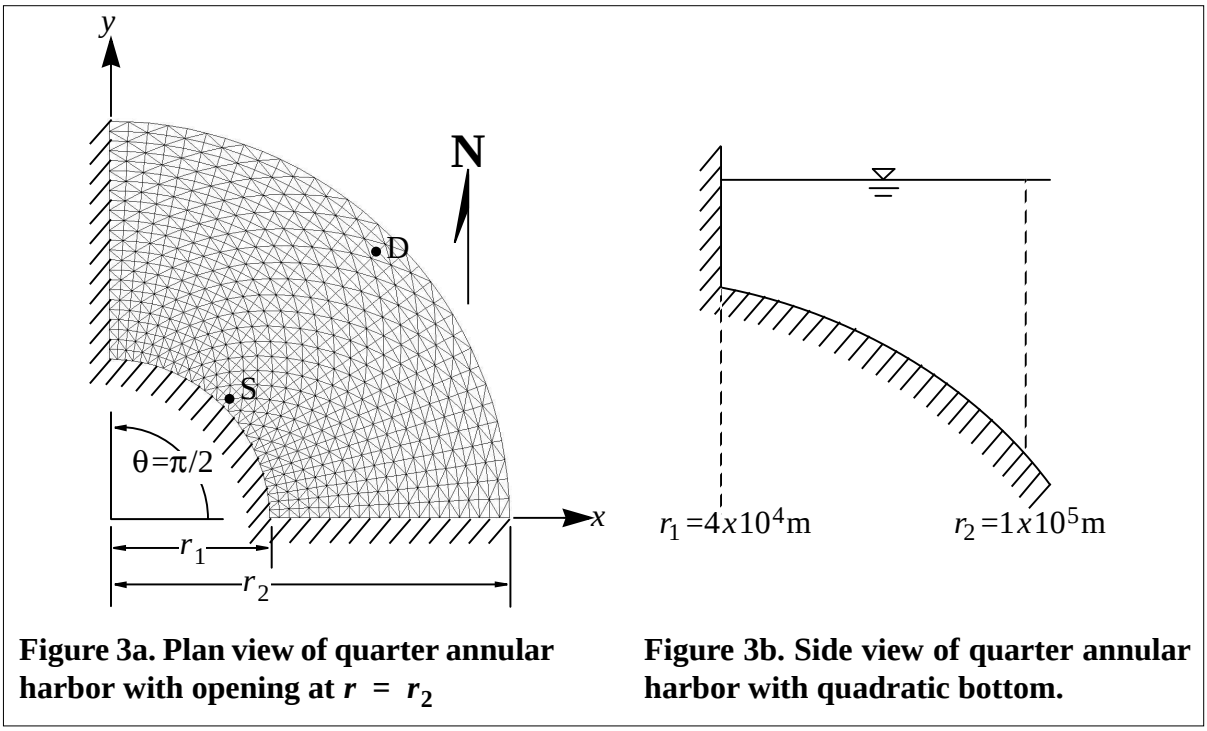

Figure 3a. Plan view of quarter annular harbor with opening at $r = r_2$

Figure 3b. Side view of quarter annular harbor with quadratic bottom.

The horizontal velocity is calculated using the analytic solution in *Lynch and Officer* (1985); the horizontal velocities are calculated analytically, rather than numerically, so that any deviations of the numeric vertical velocity solution from the analytic vertical velocity solution owe entirely to the vertical velocity solution technique, not numerical errors in the horizontal velocity.

However, evaluation of horizontal velocity *derivatives* is considered to be a component of the vertical velocity calculation procedure. Thus (20), (21) and (23) are discretized in the horizontal using Galerkin finite elements with linear basis functions. The solution is evaluated using the grid shown in Figure 3a. The grid has 825 nodes and 1536 elements in the horizontal and 32 evenly spaced sigma layers in the vertical. Results are presented here for the two representative nodes shown in the figure: Node S is shallow ($h = 11.29$ m) and Node D is deep ($h = 56.41$ m).

The results in *Muccino et al.* (1997) are for two sets of parameters, and are shown at just one instant in the tidal cycle. Here, we use one set of parameters (consistent with Figure 4 in *Muccino et al.* (1997): $\lambda = 6.627 + 6.627i$ and $K = 102.1$, see the Appendix for definition of these parameters), and present the vertical velocity as amplitude and phase in Figure 4. The parameter W_f/H^2 is set to zero here; its impact on the ADJ solution is investigated next. In these figures, the analytic, ADJ and VDC (20) amplitude and phase are coincident, with VDC (21) amplitude and phase differing from them. Results for different values of λ and K and h_0 and at other nodes are not shown but are qualitatively similar, indicating that the observations regarding Figure 4 do not depend upon particular choices of parameters or bathymetry, but rather are quite general.

Now we will consider the impact of W_f/H^2 on the ADJ solution. Recall the normalized correction profiles for various values of W_f/H^2 in Figure 1; to obtain the actual correction, these profiles are scaled by the surface boundary condition misfit of the traditional solution (9). In the

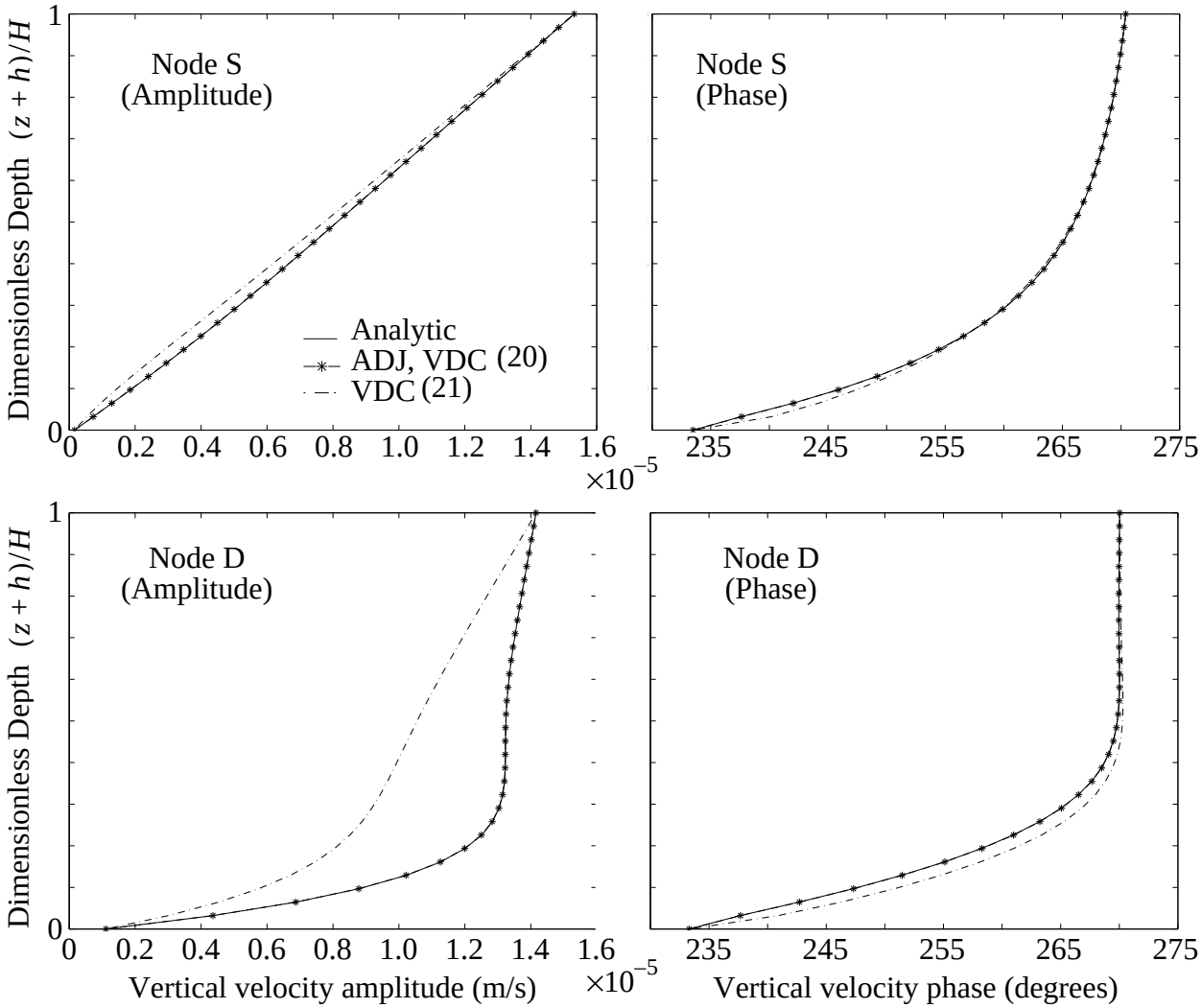

Figure 4. Amplitude and phase of vertical velocity in the quarter annular harbor at Node S and Node D. Note that the analytic, ADJ and VDC (20) solutions are coincident, but different from the VDC (21) solution.

quarter annular harbor, the magnitude of this misfit is two or three orders of magnitude smaller than w_{trad}. Thus, the ADJ correction is insignificant, regardless of the value of W_f/H^2, and ADJ essentially collapses to the traditional approach.

6. Application to the Pacific Coast of Southwest Vancouver Island.

The summer circulation off the western continental margin of Vancouver Island is characterized by a moderately intense upwelling of nutrients that supports high biological productivity

and a lucrative commercial fishery. Circulation models (e.g., *Foreman et al*. 2000) have been developed to better understand both spatial and temporal variations in this upwelling, and these physical models are now being coupled to biological models in order to simulate specific components of the food chain. The accuracy of these models is highly dependent on both their adherence to mass conservation (so that nutrients are not falsely depleted or created) and the accuracy of the vertical velocities that move nutrients and biota up the water column. A circulation model for this region is thus a useful test for the vertical velocity calculations described here.

The model used here is the pseudo-nonlinear FUNDY5 (*Lynch and Werner*, 1987) that incorporates root-mean square tidal velocities in the bottom friction and vertical viscosity coefficients (see *Foreman et al.*(2000) for further details). This model solves the three-dimensional, harmonic shallow water equations in the sequential manner described in Section 1 using linear triangular finite elements. In this test application we consider only the steady state solution resulting from steady forcing. Combined wind- and buoyancy- driven flows are forced with average winds measured at a meteorological buoy near the middle of the model domain and a three-dimensional density field that was constructed through Kriging of temperature and conductivity measurements taken in late July, 1998. Boundary conditions for these calculations were computed through a combination of geostrophic radiation conditions and adjustments to the surface elevations so that the vertically-integrated flows passed through the boundary without any reflection. Analogous to the inversion described in *Foreman et al.*(2000), further boundary condition adjustments were also made to introduce a California Undercurrent consistent with observations at two current meter moorings lying along the continental slope.

The computational grid is comprised of 9767 nodes horizontally (Figure 5) and 41 evenly spaced sigma surfaces vertically. Several nodes are highlighted in the figure for future reference;

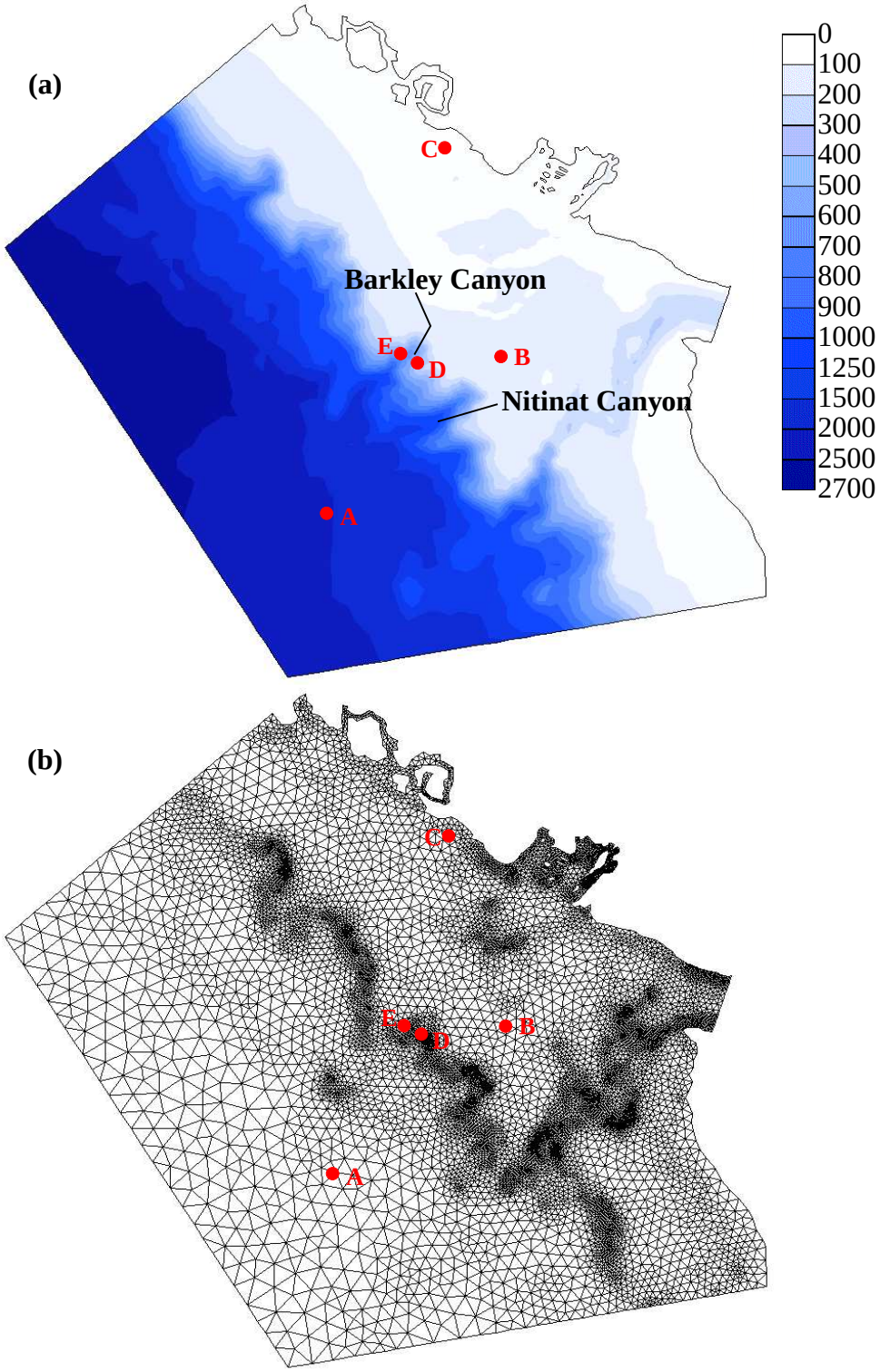

Figure 5. The Southwestern Vancouver Island domain (a) contours of bathymetry (meters); (b) computational grid. Labeled points are discussed further in the text.

Table 1. Description of representative nodes in Southwestern Vancouver Island Domain

Node	Region	H (m)	Surface BC misfit of traditional solution (m/s)
A	Deep Ocean	2020	-6.0×10^{-5}
B	Continental Shelf	138	-6.7×10^{-5}
C	Coast	35	-1.5×10^{-7}
D	South Barkley Canyon	475	-1.4×10^{-3}
E	North Barkley Canyon	487	6.2×10^{-3}

each of these nodes is representative of certain regions in the domain, as detailed in Table 1. Vertical velocity profiles for Nodes A through E calculated with ADJ and a range of W_f/H^2 values and VDC (21) are shown in Figure 6. Since, the VDC (20) solution is coincident with the ADJ solution when $W_f/H^2 = 0$, it is not distinct in Figure 6. Several observations may be made regarding these figures:

1. In all cases, the VDC (21) solution is substantially different than the ADJ solutions for any value of W_f/H^2.
2. In the deep ocean (Node A), on the continental shelf (Node B) and near the coast (Node C), the vertical velocities are very small (order 1×10^{-5}m/s).
3. Along the sides of Barkley Canyon (Nodes D and E), the vertical velocities are one to two orders of magnitude greater than at Nodes A, B and C. The ability to predict the patterns of vertical velocity in regions such as Barkley Canyon is important in understanding biological productivity (*Allen et al.*, 2001). Of particular concern here is the fact that VDC (21) and ADJ predict opposite vertical velocity trends. On the south side

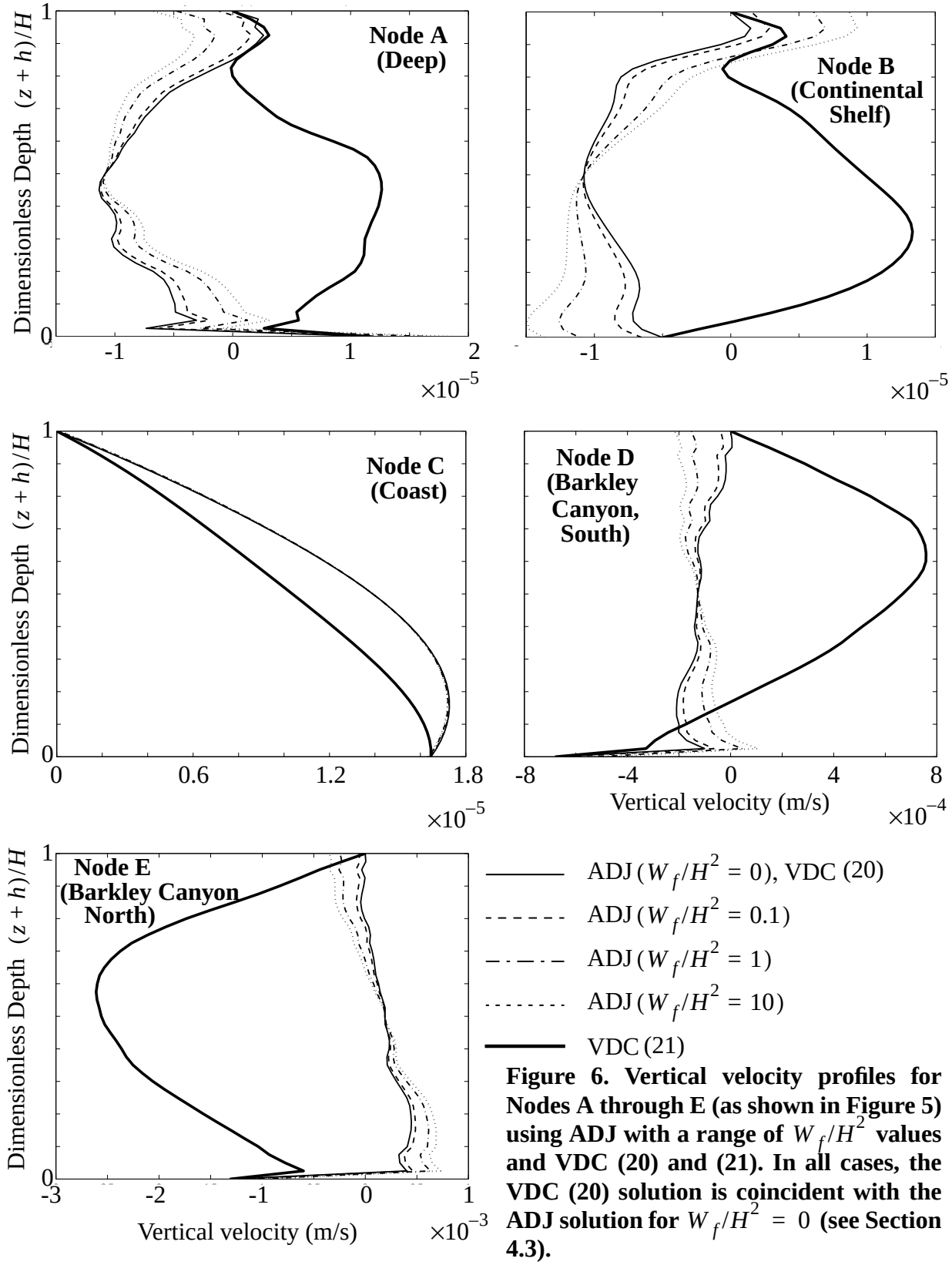

Figure 6. Vertical velocity profiles for Nodes A through E (as shown in Figure 5) using ADJ with a range of W_f/H^2 values and VDC (20) and (21). In all cases, the VDC (20) solution is coincident with the ADJ solution for $W_f/H^2 = 0$ (see Section 4.3).

of Barkley Canyon, VDC (21) predicts upwelling while ADJ predicts downwelling, and on the north side of the same canyon, VDC (21) predicts downwelling while ADJ predicts upwelling. Further insight into the vertical velocity behavior may be gained by examining the horizontal velocity field in that region at $z = -300$ m ($(z + h)/H \approx 0.4$ at Nodes D and E) as illustrated in Figure 7; this figure shows a California Undercurrent that generally follows the bathymetry towards the northwest. However, the flow cuts across the deepest parts of the canyon, suggesting downwelling on the south side of the canyon and upwelling on the north side of the canyon. This is the vertical velocity behavior predicted by ADJ for all values of W_f/H^2; VDC (21) predicts the opposite.

4. Unlike results presented for the quarter annular harbor, there is considerable dependence here of the ADJ solution on W_f/H^2 for all nodes except near the coast at Node C. This dependence indicates that the surface boundary condition misfit of the traditional solution is relatively large.
5. As shown in Figure 1, there is not much change in the vertical velocity solution obtained with values of $W_f/H^2 = 10$ and $W_f/H^2 = 100$, and thus we consider these values of W_f/H^2 to be "large" in the sense that larger values will not substantially change the solution. Likewise, there is little difference in the solution obtained with values of $W_f/H^2 = 0$ and $W_f/H^2 = 0.1$, and thus we consider these values of W_f/H^2 to be "small."

7. Effects of local mass conservation

The previous sections have shown that the traditional, adjoint and vertical derivative (20) solutions for vertical velocity give essentially identical results when the surface boundary condition misfit of the traditional solution is equal to zero. This misfit is readily identified as owing to errors

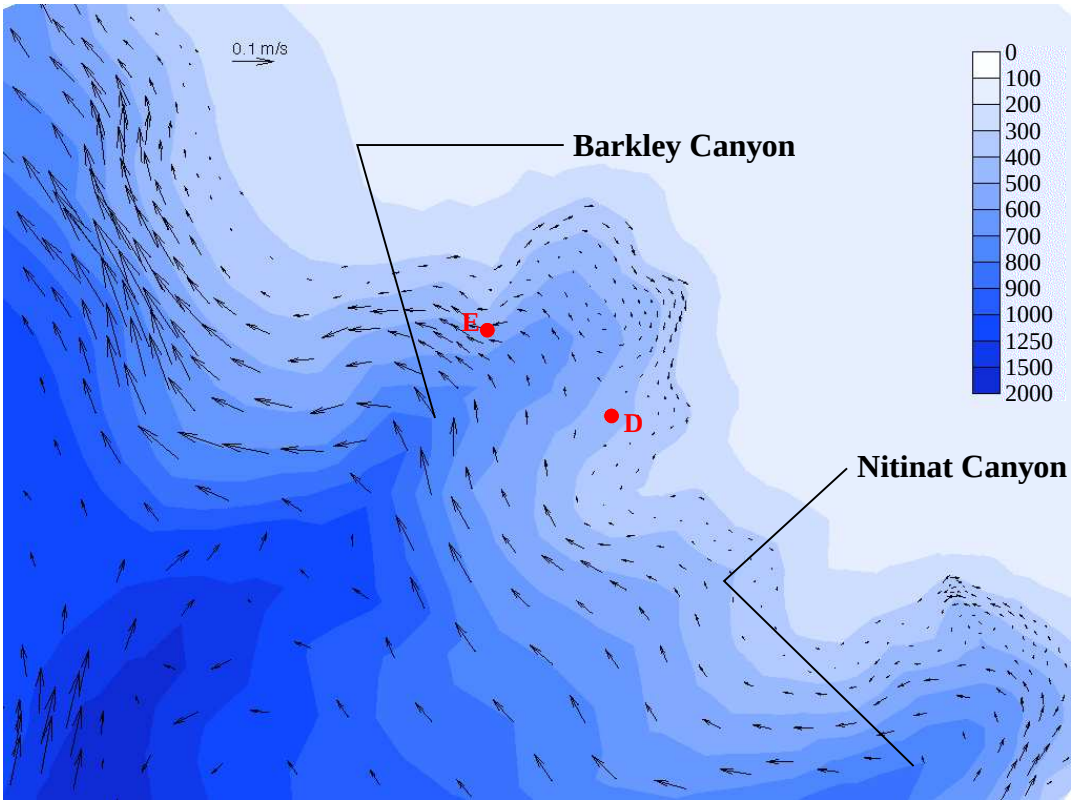

Figure 7. Horizontal velocity field at z=-300 m (velocities on stretched coordinate surfaces are interpolated onto the level surface 300 m below the surface). The flow is towards the northwest largely following the bathymetry. However, the flow cuts across the deepest part of the Barkley Canyon; this would indicate a downwelling on the south side of the canyon and an upwelling on the north side of the canyon.

in the horizontal solution. Integrating (1) from the bottom upward and applying the bottom boundary condition (2a) yields:

$$w_{trad}(z) = -\int_{-h}^{z} \nabla \cdot \mathbf{V} dz - \mathbf{V}(-h) \cdot \nabla h \tag{28}$$

Applying Liebnitz's Rule to the integral in (28) yields:

$$w_{trad}(z) = -\nabla \cdot \int_{-h}^{z} \mathbf{V} dz + \mathbf{V}(z) \cdot \nabla z \tag{29}$$

In the interior of the water column, $\nabla z = 0$ and the vertical velocity is simply the horizontal divergence of the horizontal velocity field integrated up from the bottom. At the free surface, (29) becomes:

$$w_{trad}(\eta) = -\nabla \cdot \int_{-h}^{\eta} \mathbf{V} dz + \mathbf{V}(\eta) \cdot \nabla \eta \tag{30}$$

Using the surface boundary condition (2b) to replace the final term in (30) and rearranging gives:

$$w_s - w_{trad}(\eta) = \frac{\partial \eta}{\partial t} + \nabla \cdot \int_{-h}^{\eta} \mathbf{V} dz \tag{31}$$

The RHS of (31) is the vertically-integrated continuity equation. Consequently, (31) shows that the misfit between the traditional solution evaluated at the surface and the surface boundary condition is nonzero anywhere in the domain that the horizontal velocity field does not conserve mass in the vertically-integrated sense. Since numerical models solve discrete rather than continuous governing equations, discretization of the vertically-integrated continuity equation in (31) must match that used to evaluate (1), (2a) and (2b).Thus, local mass conservation, on the same numerical stencil used to determine w, is required if the misfit on the LHS of (31) is to be zero. If mass is not locally conserved, error is introduced into the computed vertical velocity field as it is integrated up the water column.

The quarter annular test problem presented in Section 5 uses horizontal velocities obtained from the analytical solution and thus these velocities satisfy the vertically-integrated continuity equation exactly; the surface misfit is insignificant and VDC (20) and ADJ with any value of the parameter W_f/H^2 give essentially identical results throughout the domain.

While finite difference models using Arikawa C grids conserve mass on each computational cell, Galerkin finite element models are guaranteed to conserve mass only globally (*Lynch*, 1985; *Lynch and Holboke*, 1997) and therefore allow for nonzero local residuals in the vertically-integrated continuity equation. Figure 8 illustrates the surface misfits for the Vancouver Island test problem; by (31), this plot also represents local vertically-integrated continuity residuals. Considerable surface misfits are observed; areas having large misfits (and thus poor vertically-integrated mass conservation) typically correspond to areas of steep bathymetric gradients. Plots of surface misfits or vertically-integrated mass error such as this are easy to construct and provide a useful diagnostic tool for identifying areas where local mass conservation is relatively poor, and therefore where significant errors are likely to exist in the vertical velocity solution.

As outlined earlier, most oceanic circulation models follow a sequential solution procedure in which the vertical velocity solution occurs separate from and with minimal feed back to the horizontal velocity solution. Since mass conservation error in the horizontal solution is the cause of the vertical velocity solution error identified above, it seems inadvisable to sacrifice the boundary condition information in favor of stricter adherence to the three-dimensional continuity equation when determining the vertical velocity. Consequently, we suggest a small value of the ADJ weighting parameter W_f/H^2 ($W_f/H^2 < 0.1$) as preferable to a high value ($W_f/H^2 > 10$).

8. Conclusions

The results presented in this paper help reconcile past uncertainty in the vertical velocity solution in three-dimensional circulation models. Specifically, we have found the following.

1. Most three-dimensional circulation models use a sequential solution procedure to solve for the free surface elevation and velocity fields. That is, the vertically-integrated conti-

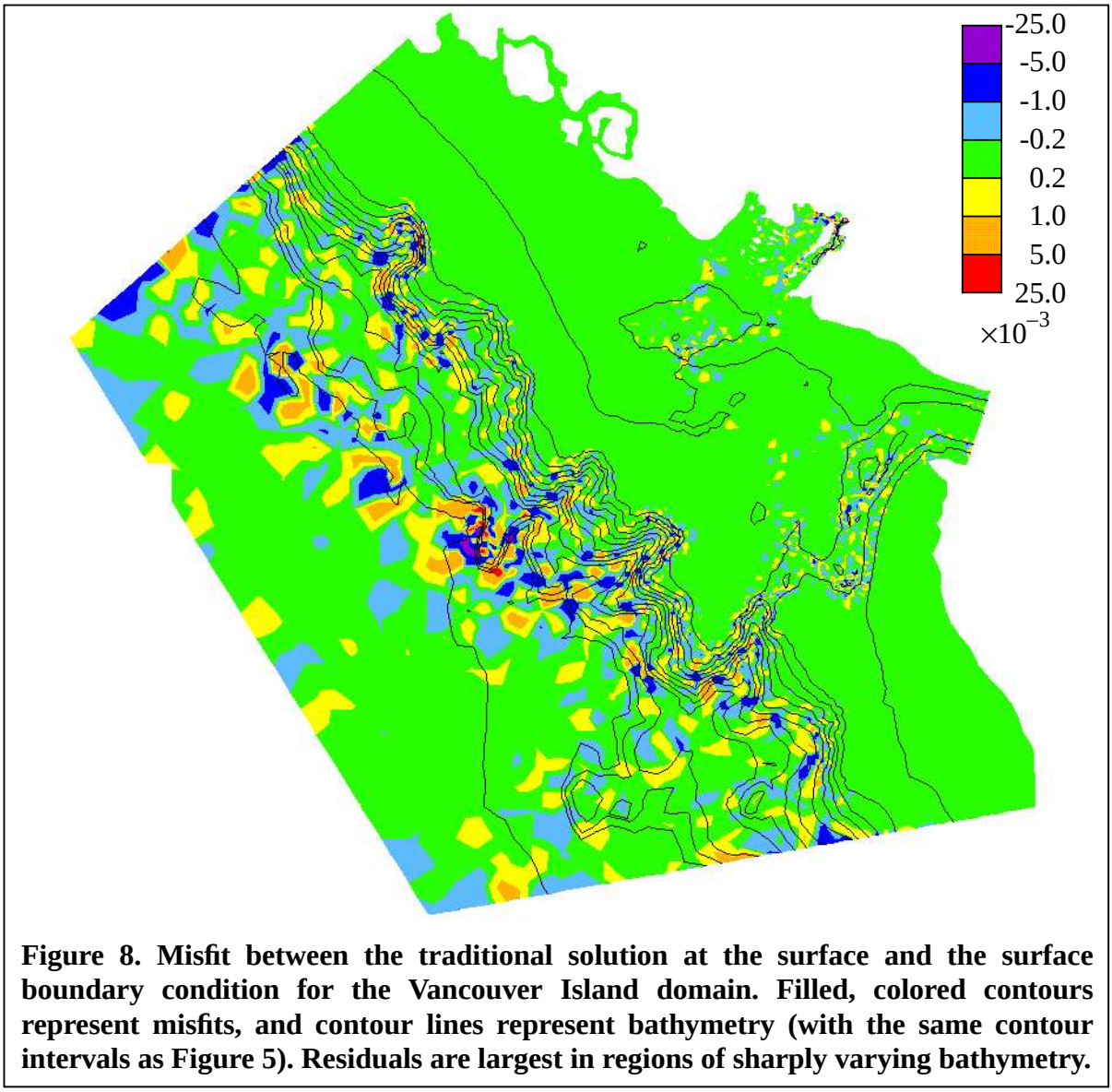

Figure 8. Misfit between the traditional solution at the surface and the surface boundary condition for the Vancouver Island domain. Filled, colored contours represent misfits, and contour lines represent bathymetry (with the same contour intervals as Figure 5). Residuals are largest in regions of sharply varying bathymetry.

nuity and the three-dimensional momentum equations are solved first for the free surface elevation and the horizontal velocity fields; then the three-dimensional continuity equation is solved for the vertical velocity field. Solving the three-dimensional continuity equation (a first order differential equation in the vertical coordinate) for the vertical velocity would appear to be problematic given the need to satisfy boundary conditions at both the bottom and at the free surface. However, the “traditional”

(TRAD) vertical velocity solution, obtained by integrating the three-dimensional continuity equation upward using the bottom boundary condition, will match the surface boundary condition if the elevation and horizontal velocity fields exactly satisfy the vertically-integrated continuity equation. In this case, the surface boundary condition is redundant. If the elevation and horizontal velocity fields are not locally mass conserving, the misfit between the TRAD solution and the surface boundary condition is equal to the local error in the vertically-integrated continuity equation.

2. The VDC approach proposed by *Lynch and Naimie* (1993), in which the vertical velocity is computed from the vertical derivative of the three-dimensional continuity equation, is equivalent to an optimal, adjoint solution (ADJ) of the three-dimensional continuity equation (*Muccino et al.*, 1997) in which the boundary conditions are preserved in lieu of stricter adherence to the continuity equation. VDC requires the solution of a tri-diagonal matrix problem over the vertical while ADJ requires no matrix solution. Thus ADJ is more computationally efficient than VDC.
3. Depending upon the numerical discretization applied to VDC, results are obtained that are less accurate than the other vertical velocity solutions in the quarter annular harbor test case and that appear to be physically inconsistent in the Vancouver Island test case. We recommend that if VDC is used, the discretization presented in (20) be used rather than the discretization presented in (21).
4. The ADJ solution is the solution that minimizes the cost functional (5) which penalizes misfits to the three-dimensional continuity equation and the misfits of the bottom and surface boundary conditions. The ADJ solution can be shown to be the sum of the TRAD solution and a linear correction. In the limit of satisfying both the bottom and

free surface boundary conditions ($W_f/H^2 = 0$) the correction is zero at the bottom and equal to the misfit of the TRAD solution and the free surface boundary condition at the surface. In the limit of maximizing adherence to the three-dimensional continuity equation, $W_f/H^2 > 10$, the correction is a constant over the entire water column and equal to one half of the misfit of the TRAD solution and the free surface boundary condition.

5. If there is no misfit between the TRAD solution and the free surface boundary condition, TRAD, ADJ and VDC (20) give identical solutions for the vertical velocity.
6. Results from models that do not enforce strict local mass conservation, such as finite element models, will be susceptible to the vertical velocity errors described herein. We recommend plotting maps of the error in the vertically-integrated continuity equation as a diagnostic tool for determining areas in the domain that may be subject to significant vertical velocity errors. The first choice for improving the computed vertical velocity is to reduce errors in vertically-integrated mass conservation, either by improved grid resolution or by smoothing the bathymetry (*Oliveira et al.*, 2000). Mass conservation may also be improved in Generalized Wave Continuity Equation based finite element models by increasing the primitive continuity equation weighting parameter (known as τ_0 or G), (*Kolar et al.*, 1992, 1994). If local mass conservation cannot be achieved, we suggest use of ADJ with the weighting coefficient set to preferentially favor the surface and bottom boundary conditions ($W_f/H^2 < 0.1$).

9. Acknowledgements

The authors would like to thank Chris Naimie for independently confirming that the results presented here are consistent with FUNDY5. The authors also thank Rick Thomson, Susan Allen, Dave Mackas and the crew of the CCGS *John P. Tully* for collecting the salinity, temperature, and

velocity data that were used in this study. These observations were taken during a GLOBEC Canada cruise that was co-sponsored by the Natural Sciences and Engineering Research Council of Canada and the Department of Fisheries and Oceans. R. Luettich would like to acknowledge partial funding for this work by the Office of Naval Research award N00014-97-C-6010 and J. Muccino would like to acknowledge partial funding for this work by the National Science Foundation under OCE-9520956.

10. Appendix: Analytic solution quarter annular harbor

Consider a quarter annular harbor with no-flow boundaries at $r = r_1$, $\theta = 0$, and $\theta = \pi/2$ and an open boundary at $r = r_2$. The open boundary is subject to periodic forcing $\eta = Re\{\eta_0 e^{i\omega t}\}$. The bathymetry of the harbor is quadratic in r and constant in θ, such that $h = h_0 r^2$. The eddy viscosity, N, and bottom friction, k, vary such that:

$$K = \frac{kh}{N} \quad \text{and} \quad \lambda = \sqrt{\frac{i\omega h^2}{N}}, \tag{32}$$

are constant. The analytic solution for surface elevation and horizontal velocity (*Lynch and Officer*, 1985) are:

$$\eta(r,t) = Re\left\{(Ar^{s_1} + Br^{s_2})\exp(i\omega t)\right\} \tag{33}$$

$$v(r,\sigma,t) = Re\{v_0(r)(1-\delta\cosh(\lambda\sigma))e^{i\omega t}\} \tag{34}$$

where: $A = \dfrac{\eta_0 s_2 r_1^{s_2}}{s_2 r_2^{s_1} r_1^{s_2} - s_1 r_1^{s_1} r_2^{s_2}}$, $B = \dfrac{-\eta_0 s_1 r_1^{s_1}}{s_2 r_2^{s_1} r_1^{s_2} - s_1 r_1^{s_1} r_2^{s_2}}$

$s_1 = -1 + \sqrt{1-\beta^2}$, $\quad s_2 = -1 - \sqrt{1-\beta^2}$

$\beta^2 = (\omega^2 - i\omega\tau)/(gh_0)$

$$\tau = \frac{N}{h^2}\left[\frac{\lambda^2 \tanh\lambda}{\lambda + \left(\frac{\lambda^2}{K} - 1\right)\tanh\lambda}\right]$$

$$v_0(r) = -\frac{g}{i\omega r}(s_1 A r^{s_1} + s_2 B r^{s_2})$$

g is the gravitational constant and $i = \sqrt{-1}$. The vertical velocity is (*Muccino et al.*, 1997):

$$w(r, \sigma, t) = Re\left\{\left(2\gamma\alpha_1\delta\left[(\sigma\cosh(\lambda\sigma) + \cosh(\lambda)) - \frac{\sinh(\lambda\sigma) + \sinh(\lambda)}{\lambda}\right]\right.\right.$$

$$\left.\left. + \gamma\alpha_2\left[\sigma + 1 - \frac{\delta(\sinh(\lambda\sigma) + \sinh(\lambda))}{\lambda}\right] + 2\gamma\alpha_1[1 - \delta\cosh(\lambda)]\right)e^{i\omega t}\right\} \qquad (35)$$

where: $\sigma = z/h$

$$\gamma = \frac{gh_0}{i\omega}\exp(i\omega t)$$

$$\alpha_1 = As_1 r^{s_1} + Bs_2 r^{s_2}, \quad \alpha_2 = As_1^2 r^{s_1} + Bs_2^2 r^{s_2}$$

$$\delta = \frac{1}{\cosh(\lambda)\left[1 + \frac{\lambda}{K}\tanh(\lambda)\right]}$$

11. References

Allen, S. E., C. Vindeirinho, R. E. Thomson, M. G. G. Foreman and D. L. Mackas, 2001: Physical and biological processes over a submarine canyon during an upwelling event. *Canadian Journal of Fisheries and Aquatic Sciences*, **59**(4), 671-684.

Blumberg, A. F. and G. L. Mellor, 1987: A description of a three-dimensional coastal ocean circulation model. In: C.N.K. Mooers, [ed], *Three-dimensional Coastal Ocean Models*, Coastal and Estuarine Sciences 4, AGU Press, Washington, DC, 1-16.

Foreman, M. G. G., R. E. Thomson, and C. L. Smith, 2000: Seasonal current simulations for the western continental margin of Vancouver Island. *J. Geophys. Res.*, **105**(C8), 19,665-19,698.

Haidvogel, D.B. and A. Beckmann. 1999: Three-dimensional ocean models. Chapter 4 in *Numerical Ocean Circulation Modeling*, Imperial College Press, London, England, 121-162.

Kolar, R. L., W. G. Gray, J. J. Westerink and R. A. Luettich, Jr., 1994: Shallow water modeling in spherical coordinates: Equation formulation, numerical implementation and application. *J. Hydraul. Res.*, **32**(1), 3-24.

Kolar, R. L., W. G. Gray and J. J. Westerink, 1992: An analysis of the mass conserving properties of the generalized wave continuity equation. *Computational Methods in Water Resources IX*, **2**, T. Russell et al., [eds], Computational Mechanics Publications, Southampton, UK, pp. 537-544.

Lynch, D.R. and M.J. Holboke, 1997: Normal flow boundary conditions in 3D circulation models. *Int. J. Numer. Meth. Fluids*, **25**, 1185-1205.

Lynch, D. R. and C. E. Naimie, 1993: The M2 tide and its residual on the outer banks of the Gulf of Maine. *J. Phys. Oceanogr.*, **23**, pp. 2222-2253.

Lynch, D. R. and F. E. Werner, 1991: Three-dimensional hydrodynamics on finite elements. Part I: Nonlinear time-stepping model. *Int. J. Numer. Meth. Fluids*, **12**, 507-533.

Lynch, D. R. and F. E. Werner, 1987: Three-dimensional hydrodynamics on finite elements. Part II: Linearized harmonic model. *Int. J. Numer. Meth. Fluids*, **7**, 871-909.

Lynch, D. R. and C. B. Officer, 1985: Analytic test cases for three-dimensional hydrodynamic models. *Int. J. Numer. Meth. Fluids*, **5**, 529-543.

Lynch, D. R., 1985: Mass balance in shallow water simulations. *Communications in Applied Numerical Methods*, **1**, 153-159.

Muccino, J.C. and A. F. Bennett, 2001: Generalized inversion of the Korteweg-de Vries Equation. submitted to *Dyn. Atmos. Oceans*.

Muccino, J. C., W. G. Gray and M. G. G. Foreman, 1997: Calculation of vertical velocity in three-dimensional, shallow water equation, finite element models. *Int. J. Numer. Meth. Fluids*, **25**, 779-802.

Oliveira, A., A. B. Fortunato and A. M. Baptista, 2000: Mass balance in Eulerian-Lagrangian transport simulations in estuaries. *J. Hydraul. Eng.*, **126**, 605-614.